Petrogenesis of late Mesozoic high-Ba–Sr granites in the Qiushuwan Cu Mo orefield: Implications for the distribution of porphyry Mo mineralization in the East Qinling area of Centr…

Article *in* Lithos · August 2019

DOI: 10.1016/j.lithos.2019.105172

3 authors, including:

Zhiwei Bao
Chinese Academy of Sciences
84 PUBLICATIONS **2,690** CITATIONS

SEE PROFILE

Lithos 348–349 (2019) 105172

Contents lists available at ScienceDirect

Lithos

journal homepage: www.elsevier.com/locate/lithos

Petrogenesis of late Mesozoic high-Ba–Sr granites in the Qiushuwan Cu—Mo orefield: Implications for the distribution of porphyry Mo mineralization in the East Qinling area of Central China

Zhiwei Bao [a,*], Mingfu Xiong [a,b], Qun Li [a,b]

[a] Key Laboratory for Mineralogy and Metallogeny, Guangzhou Institute of Geochemistry, Chinese Academy of Sciences, Guangzhou 510640, China
[b] University of Chinese Academy of Sciences, Beijing 100049, China

ARTICLE INFO

Article history:
Received 19 March 2019
Received in revised form 9 August 2019
Accepted 11 August 2019
Available online 19 August 2019

Keywords:
High-Ba–Sr granite
North Qinling
Enriched subcontinental lithospheric mantle
Porphyry Cu—Mo mineralization
East Qinling orogenic belt

ABSTRACT

The Qinling–Dabie orogenic belt of China is well known for its large Mo resources. There have been many studies of the genesis of the Mo deposits, but the reasons for the intensive mineralization during the late Mesozoic and the spatially uneven distribution of the resulting ore deposits are not fully understood. Deposits with reserves of >6 Mt. of Mo occur predominantly in the southern margin of the North China Craton (NCC) and are mostly late Mesozoic porphyry deposits. In comparison, a few relatively insignificant and Cu-dominated porphyry ore deposits have been identified in the North and South Qinling terranes. This study presents new whole-rock geochemical, isotopic, and zircon U—Pb age data for ore-bearing granites associated with the Qiushuwan Cu—Mo deposit, the largest porphyry deposit in the North Qinling (NQ) terrane, which provide insights into the asymmetric distribution of Mo mineralization in this region. The rocks display high-K calc-alkaline to shoshonitic affinities, and are metaluminous to weakly peraluminous with high Ba and Sr contents, low Rb, Nb, and Ta contents, and depletion in heavy rare earth elements and Y, which are features typical of high-Ba–Sr granites. Zircon U—Pb dating indicates that the granites crystallized at *ca* 145 Ma. Their narrow ranges of whole-rock initial $^{87}Sr/^{86}Sr$ ratios (0.7056–0.7069) and $\varepsilon_{Nd}(t)$ (−7.4 to −9.7), zircon $\varepsilon_{Hf}(t)$ (−2.49 to −5.13), and $\delta^{18}O$ (+5.58‰ to +6.49‰) values, together with the presence of significant Nd—Hf isotopic decoupling (Δ_{Hf} = +7.61 to +11.3), indicate that the parent magma was derived from partial melting of enriched subcontinental lithospheric mantle with minor assimilation of the lower crust. In contrast, late Mesozoic granitic rocks in the southern margin of the NCC (including both mineralized and barren intrusions) are geochemically associated with the crust of the northern margin of the Yangtze Block (YB). The YB contains Mo-rich shales that are thought to have been subducted beneath the southern margin of the NCC during the Triassic. Melting of these Mo-rich black shales would have mobilized Mo, a process that enabled the formation of the extensive Mo mineralization associated with the late Mesozoic granites of the southern margin of the NCC. This indicates that the extensive Mo mineralization within the southern margin of the NCC is genetically related to a Mo-rich source that was generated by the stagnation of subducted YB continental crust beneath the southern margin of the NCC. In comparison, the less significant Mo mineralization within the East Qinling orogenic belt might reflect the variable removal of the subducted YB continental slab during post-collisional intracontinental orogenesis.

1. Introduction

The East Qinling region, bounded by the North China Craton (NCC) to the north and Yangtze Block (YB) to the south, is part of the Central China Orogenic Belt (CCOB) that extends for >4000 km from West Kunlun in the west, through Qilian, West Qinling, East Qinling, and Dabie, to Sulu in the east (Dong and Santosh, 2016; Wu and Zheng, 2013). The region is well known for its >6 Mt. of Mo reserves, of which >92% are porphyry-type deposits associated with late Mesozoic (Late Jurassic–Middle Cretaceous) granites at the southern margin of the NCC (e.g., Mao et al., 2011). Only a few such deposits are found in the other terranes of this orogenic belt (Guo et al., 2006; Xie et al., 2015). The mineralization within these deposits in the southern margin of the NCC is dominated by Mo, with lesser amounts of W, Ag, Pb, and Zn, whereas those in other terranes are commonly Cu-dominated with subordinate Mo (Bao et al., 2014; Xie et al., 2017).

The inconsistent distribution of mineralization of late Mesozoic granites in the East Qinling orogenic belt (EQOB) remains to be explained. The EQOB formed as a result of the Triassic collision between the NCC and YB along the Mianlue suture (Wu and Zheng, 2013), and this area contains widespread late Mesozoic granites. All of the large

* Corresponding author.
E-mail address: baozw@gig.ac.cn (Z. Bao).

https://doi.org/10.1016/j.lithos.2019.105172
0024-4937/

porphyry (−skarn) Mo deposits identified within the EQOB to date are located within the southern margin of the NCC, with only smaller and more Cu-dominated porphyry deposits located within the other terranes in this region (Fig. 1). The reasons for this uneven distribution of mineralization remain unclear. It was generally considered that the extensive Mo mineralization in the southern margin of the NCC resulted from remelting of Mo-rich basement of Neoarchean Taihua Group metamorphic rocks (e.g., Yang et al., 2013), but studies of crustal rocks in the EQOB have shown that such basement is virtually non-existent (Gao et al., 1998). A basement-derived source is also inconsistent with the considerably younger whole-rock Nd and zircon Hf two-stage model ages of the granites and isotopically enriched signatures of Mesozoic subcontinental lithospheric mantle in the region (Bao et al., 2014). An alternative interpretation is that the granites were derived from partial melting of stagnated subducted continental YB crust, which contains abundant Mo-rich sedimentary rocks (Bao et al., 2014, 2017). Paradoxically, if the extensive late Mesozoic Mo mineralization within the southern margin of the NCC was related to recycling of subducted YB continental crustal material, then it is unclear why the contemporaneous granites within the North and South Qinling terranes, which lie between the southern margin of the NCC and the Mianlue suture along which the YB and NCC were finally amalgamated during the early Mesozoic, host less significant Mo mineralization and are instead associated with the formation of small- to moderate-sized Cu-dominated porphyry (−skarn) deposits (Guo et al., 2006; Xie et al., 2015, 2017).

It is commonly accepted that metals in porphyry ore deposits originate from the same magma source as their host granite porphyries (e.g., Hedenquist and Lowenstern, 1994). Petrogenetic investigation of the late Mesozoic granites is therefore important in elucidating the asymmetrical distribution of Mo deposits in the EQOB. The Qiushuwan Cu—Mo deposit is medium-sized, but it is the largest porphyry ore deposit related to late Mesozoic granites in the North and South Qinling terranes, even though it is much smaller than its counterparts in the southern margin of the NCC. This contribution reports a systematic petrological and geochemical study of ore-bearing granites in the Qiushuwan orefield, in order to investigate the asymmetrical distribution and diverse metal associations of porphyry ore mineralization in the EQOB.

2. Geological background, granite petrology, and associated mineralization

The EQOB comprises four geologically distinct terranes (Fig. 1): the southern margin of the NCC, North Qinling (NQ), South Qinling (SQ), and the northern margin of the YB (from north to south), separated by the deep Maochaoying, Shangdan, and Mianlue faults or sutures (Wu and Zheng, 2013). The NQ is considered to have been a discrete micro-continent during the Paleoproterozoic–early Neoproterozoic (Shi et al., 2018).

The Qiushuwan Cu—Mo deposit is one of the few small–medium-sized porphyry-type deposits related to late Mesozoic granitic magmatism in the NQ (Fig. 2). The deposit is located 15 km north of Zhenping town in southern Henan Province. It has proven reserves of 98 kt of Cu with an average grade of 0.72% and 1.66 kt of Mo with a grade of 0.12%. Tectonically, the deposit is situated at the eastern end of the EQOB, ~10 km north of the Shangdan Fault, which is the suture between the NQ and SQ.

The NQ contains Mesoproterozoic metamorphic basement overlain by Neoproterozoic–Paleozoic volcanic–sedimentary sequences. The basement comprises gneiss, amphibolite, and marble of the Qinling Group. The Qinling Group is distributed in the central part of the NQ as scattered lenticular bodies composed of biotite–plagioclase gneisses, garnet–sillimanite gneisses, mica–quartz schists, graphite-bearing marbles, and amphibolites or garnet amphibolites, along with some eclogites. Geochronological studies indicate that their protoliths were formed in the late Mesoproterozoic–Neoproterozoic (Yu et al., 2016). The overlying sequence comprises mainly late Neoproterozoic–early Paleozoic metabasalts and metasedimentary rocks of the Kuanping Group.

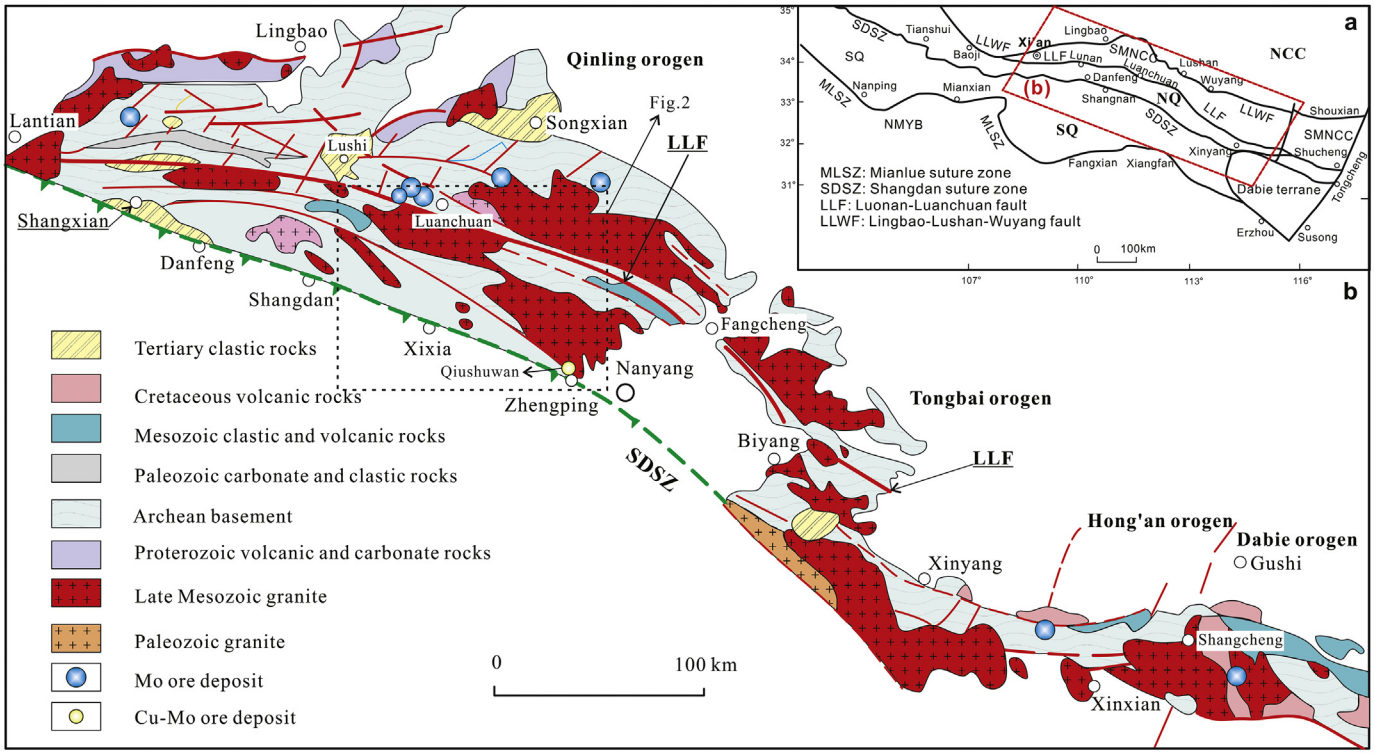

Fig. 1. Tectonic outline of the Qinling orogenic belt and a simplified geological map showing the distribution of late Mesozoic granites and related porphyry-type Mo ore deposits in the Qinling–Dabie orogenic belt.

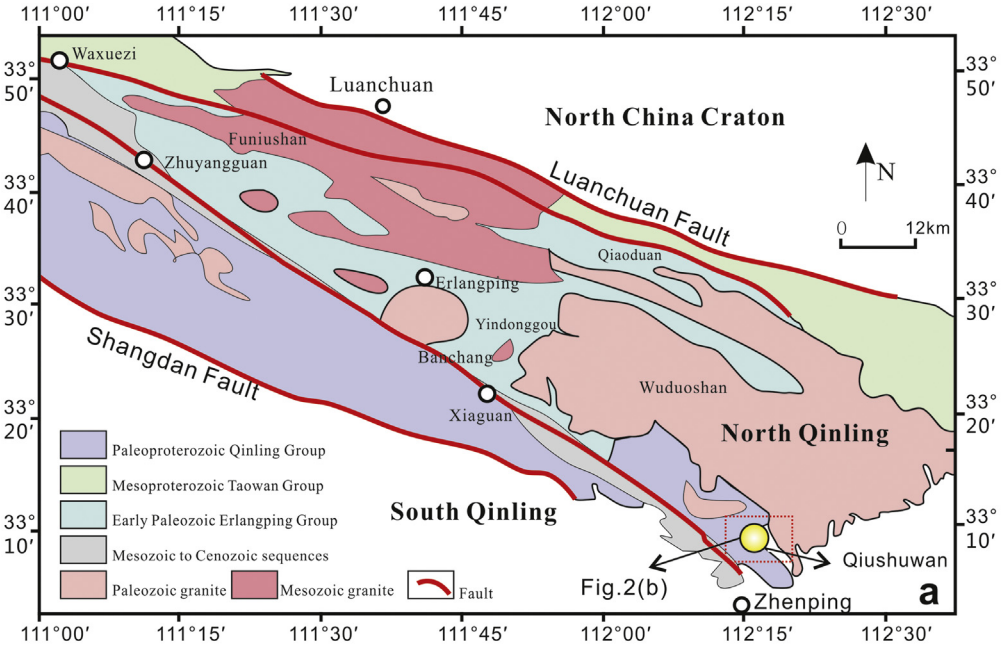

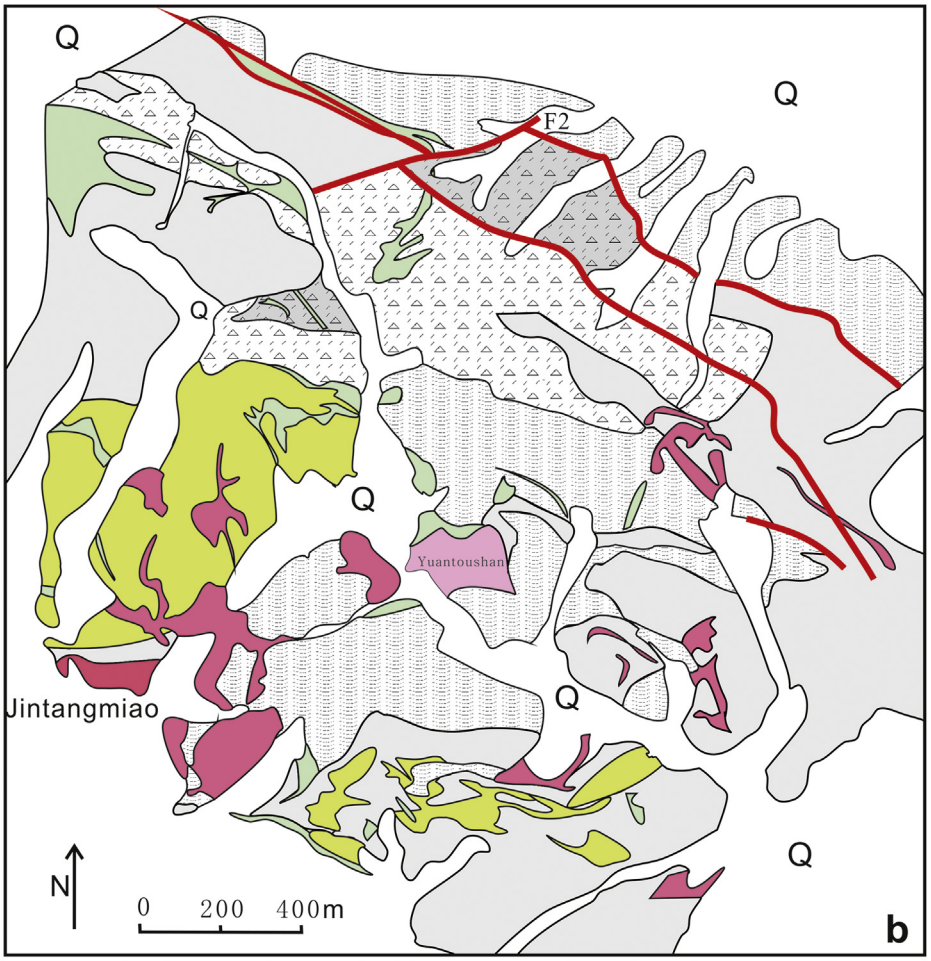

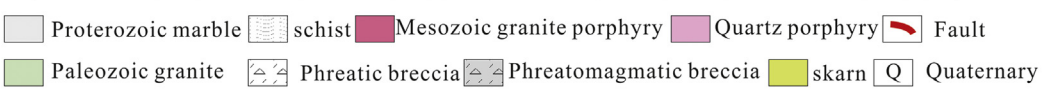

Fig. 2. Simplified geological map of the Qiushuwan porphyry Cu—Mo deposit showing (a) a tectonic outline of the eastern East Qinling orogenic belt and (b) a geological map of the Qiushuwan deposit.

Sequences cropping out in the Qiushuwan orefield include the Yanlinggou and Guozhuang formations of the Qinling Group. Rocks of the Yanlinggou Formation occur in the central to southern parts of the orefield, and consist of dolomitic marble, marble, biotite schist, and quartz–biotite schist. Granitic gneiss and marble of the Guozhuang Formation crop out in the north of the field. Igneous rocks cropping out in the orefield include the Paleozoic Wuduoshan batholith in the north (zircon U—Pb age = 439–432 Ma; Bao et al., in preparation), and a group of Mesozoic granitic porphyry stocks emplaced along the intersections of NE–SW-trending faults and WNW–ESE-trending thrust faults.

Ore-bearing granitic rocks of the Qiushuwan orefield intrude biotite gneiss, biotite–quartz schist, and marble of the Yanlinggou Formation, and occur mainly as mushroom-like stocks and irregular dikes. The granitic rocks comprise mainly porphyritic granodiorite and minor porphyritic granite (Fig. 3). The porphyritic granodiorite contains fine-grained groundmass and phenocrysts of quartz, plagioclase, K-feldspar, biotite, and minor hornblende (Fig. 3). The quartz phenocrysts commonly display resorption textures. Plagioclase consists mainly of oligoclase to andesine (An_{22}–An_{34}), with some plagioclase phenocrysts displaying zoning. K-feldspar phenocrysts are mainly orthoclase with an Al/Si ordering degree of ~0.244, indicative of very high magma temperatures, consistent with high homogenization temperatures (1050–1100 °C) of melt inclusions in quartz phenocrysts (Wang et al., 2014b). The biotite within these rocks contains high concentrations of Mg and has Mg/(Fe^{3+} + Fe^{2+} + Mg) values >0.38. Both biotite and hornblende are strongly chloritized. Accessory minerals include magnetite, apatite, titanite, zircon, ilmenite, and alanine. Highly differentiated porphyritic granite, quartz porphyry stocks, and pegmatite veins also occur in the orefield. The porphyritic granites have undergone various degrees of silicification, K-feldspathization, sericitization, and propylitization. No reliable crystallization ages have yet been reported for granitic rocks of the Qiushuwan orefield.

Orebodies in the Qiushuwan orefield include skarn-type Mo-dominated ores occurring along the southwestern contact of granitic porphyry stocks, and breccia-type Cu-dominated ores within phreatic and phreatomagmatic sub-volcanic breccias in the northeast of the field. The skarns include diopside–garnet, diopside, and garnet skarns, and comprise diopside, garnet, epidote, actinolite, hornblende, chlorite, quartz, and calcite. Breccia components comprise mainly marbles of irregular shapes and various sizes, skarn, and schist, with common granitic porphyry fragments. The breccia matrix consists mainly of skarn minerals, marble powder, and rock debris in upper levels, with crystal fragments and igneous material dominating at lower levels. Mo mineralization is mainly associated with K-feldspathization, while Cu mineralization is mainly related to sericitization. Ore minerals include chalcopyrite, molybdenite, pyrite, sphalerite, and galena, with gangue minerals of quartz, K-feldspar, sericite, calcite, epidote, garnet, and diopside. The age of Cu—Mo mineralization has been constrained to 146 ± 2 Ma through molybdenite Re—Os dating (Guo et al., 2006).

3. Analytical methods

Whole-rock major element, trace element, and Sr—Nd isotopic compositions of fresh to weakly altered porphyritic granodiorite and granite samples from the Qiushuwan orefield were analyzed at the State Key Laboratory of Isotope Geochronology and Geochemistry, Guangzhou Institute of Geochemistry, Chinese Academy of Sciences (GIGCAS). In brief, major element concentrations were determined by standard X-ray fluorescence spectrometry (XRF) of samples prepared as glass discs using a Rigaku desktop fusion machine. This approach mixed 0.50 g of rock powder previously dried at 110 °C with 4.0 g of lithium tetraborate for 15 min at 1100 °C in 95%Pt–5%Au crucibles. Analyses were performed using a Rigaku ZSX100e instrument with loss-on-ignition (LOI) measurements undertaken on samples of dried rock powder by heating in a pre-ignited silica crucible at 1000 °C for 1 h to

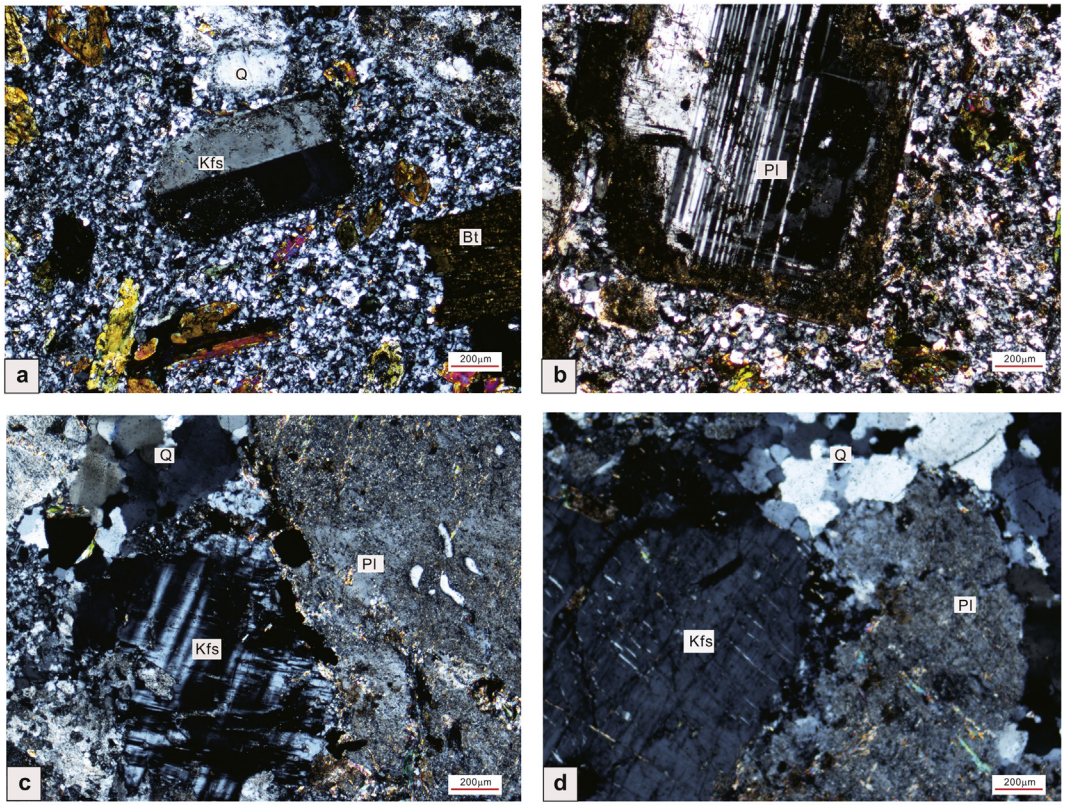

Fig. 3. Photomicrographs of the porphyritic granodiorite and granite units within the Qiushuwan orefield: (a–b) chloritized porphyritic granodiorite, (c–d) silicified and sericite altered porphyritic granite. Abbreviations are as follows: Pl = plagioclase, Bt = biotite, Kfs = K-feldspar, Q = quartz.

enable the determination of percentage weight loss. Analytical uncertainties for the XRF analysis are between 1% and 5%. Trace element concentrations were determined using inductively coupled plasma–mass spectrometry (ICP–MS) employing a Perkin-Elmer Sciex ELAN 6000 instrument. Prior to analysis, 50 mg aliquots of powdered sample were dissolved in screw-top Teflon beakers using an HF + HNO_3 mixture for 7 days at ~100 °C. An internal standard solution containing the single element Rh was used to monitor mass drift during analysis. The resulting data were calibrated using the USGS standard BCR-1. The in-run analytical precision for most elements is better 2%. The Nd isotopic compositions of the samples were determined using multicollector–ICP–MS (MC–ICP–MS) employing a Micromass Isoprobe instrument. Prior to analysis, Nd fractions were separated using cation and HDEHP columns with the resulting aqueous sample solution taken up in 2% HNO_3 and introduced into the MC–ICP–MS instrument using a Meinhard glass nebuliser with an uptake rate of 0.1 ml/min. The inlet system was cleaned for 5 min between analyses using high-purity 5% HNO_3 followed by a 2% HNO_3 blank solution. Measured $^{143}Nd/^{144}Nd$ ratios were normalized to a $^{146}Nd/^{144}Nd$ value of 0.7219 and reported $^{143}Nd/^{144}Nd$ ratios were further adjusted relative to the Shin Etsu JNdi-1 standard value of 0.512115, corresponding to the La Jolla standard of 0.511860 (Tanaka et al., 2000). Further details of the procedures used during this study are given by Li et al. (2000).

Zircons were extracted from fresh porphyritic granodiorite (sample Q1401) and weakly silicified porphyritic granite (sample Q8011) by conventional heavy liquid and magnetic techniques, and handpicked under a binocular microscope. Together with standard zircons (TEMORA), they were mounted in epoxy resin discs and polished to reveal internal structures. Cathodoluminescence (CL) images of the zircon crystals were obtained at GIGCAS using a JEOL JXA-8100 electron microprobe equipped with a Gatan Mono CL3 system.

U—Pb dating of zircon crystals from the porphyritic granite were performed using a sensitive high-resolution ion microprobe (SHRIMP II) at the Beijing SHRIMP Center, Institute of Geology, Chinese Academy of Geological Sciences, with procedures similar to those described by Williams (1998), using a spot diameter of ~25 μm and primary O_2^- ion beam intensity of 9 nA. Each spot was rastered for 150 s prior to analysis. Zircon standards SL13 (age = 572 Ma; U = 238 ppm) and TEMORA 1 (age = 417 Ma) were also analyzed (Black et al., 2003; Williams, 1998). Common Pb corrections were based on measured ^{204}Pb contents.

U—Pb dating and trace element analysis of zircons from the porphyritic granodiorite were performed by laser ablation ICP–MS (LA–ICP–MS) using an Agilent 7500a ICP–MS coupled to a Resonetics RESOlution M-50193 nm LA system at GIGCAS, with operating conditions and data processing similar to those described by Li et al. (2000). This analysis used a beam energy of 80 mJ and a beam diameter of 31 μm, with a laser repetition rate of 10 Hz. Helium was used as a carrier gas and a 417 Ma TEMORA zircon (Black et al., 2003) was used for standardization. The integration of background and analytical signals, drift corrections, and trace element calibrations were all undertaken using the GLITTER 4.0 software package (Macquarie University) and the resulting analytical data were reduced, calculated, and plotted using Isoplot 3.0 (Ludwig, 2003).

Lu—Hf isotopic analyses of zircons from the porphyritic granodiorite were undertaken with a Neptune Plus MC–ICP–MS with a RESOlution M-50-LR LA system (ArF excimer; 193 nm wavelength) at GIGCAS, with analytical procedures following those of Wu et al. (2006). A Penglai standard zircon was used as a reference material (Li et al., 2010b) and yielded a mean $^{176}Hf/^{177}Hf$ value of 0.282882 ± 0.000006 (2σ; n = 56). The laser beam energy, spot diameter, and repetition rate were 80 mJ, 33 μm, and 8 Hz, respectively.

Oxygen isotopic compositions of zircons from the porphyritic granodiorite were determined using a Cameca IMS 1280HR ion microprobe at GIGCAS, with analytical procedures similar to those of Li et al. (2010a). Isotopic data were corrected for instrumental mass fractionation using 91,500 ($\delta^{18}O_{VSMOW}$ = 9.9‰) and Penglai ($\delta^{18}O_{VSMOW}$ = 5.3‰) zircon standards (Li et al., 2010b; Wiedenbeck et al., 2004). Internal precisions for single analyses were better than ±0.20‰ (1σ). External precision, measured by the reproducibility of repeated analyses of Penglai and Qinghu standards (Li et al., 2013), was ±0.32‰ (2σ; n = 20).

4. Analytical results

4.1. Major and trace elements

The porphyritic granodiorite samples from the study area are alkali-rich ($K_2O + Na_2O$ = 7.05–8.50 wt%) and contain SiO_2 and Al_2O_3 concentrations of 59.20–64.00 and 15.30–19.65 wt%, respectively (Supplementary Table 1). In comparison, the porphyritic granite samples contain relatively high concentrations of SiO_2 (79.64–80.94 wt%) but have relatively low total alkali contents ($K_2O + Na_2O$ = 4.02–5.13 wt%). All of the samples plot in the high-K calc-alkaline and shoshonite fields on a K_2O–SiO_2 diagram (Fig. 4; Le Maitre et al., 1989). Plotting these samples in Fe-index [FeO/(FeO + MgO)] vs. SiO_2 and A/NK–A/CNK (A/NK = $Al_2O_3/Na_2O + K_2O$ molar; A/CNK = $Al_2O_3/CaO + Na_2O + K_2O$ molar) diagrams (Fig. 5a, b) indicates they are magnesian (Frost and Frost, 2008) and metaluminous to weakly peraluminous. Magnesian rocks such as those in the study area are formed by differentiation under oxidizing and relatively hydrous conditions (Frost and Frost, 2008), with the hydrous nature of these magmas also evidenced by the presence of widespread phreatic breccias in the study area, which formed as a result of crypto-explosions during the shallow intrusion of these hydrous magmas (Burnham, 1985; Fig. 2b). The samples from the study area have aluminum saturation index (ASI) values that positively correlate with SiO_2, whereas Al_2O_3, CaO, and P_2O_5 concentrations all negatively correlate with SiO_2 concentrations (Fig. 5c–f), similar to trends expected for typical I-type granites (Chappell and White, 1992).

The porphyritic granodiorite and granite rocks are characterized by enrichment in large-ion lithophile elements (LILE) such as Rb, Sr, Ba, U, and Th, and the light rare earth elements (LREE), and significant depletions in high-field-strength elements (HFSE) such Nb, Ta, Zr, and Hf (Supplementary Table 1). The rocks have high Sr and Ba contents of 929–1803 and 1300–3250 ppm, respectively (Supplementary Table 1). The variations in major and trace element concentrations relative to SiO_2 (Fig. 5) might not simply reflect fractional crystallization. The fractional crystallization of apatite, feldspar, and biotite results in negative correlations between Sr or Ba and SiO_2 as a result of the high partition coefficients for Sr in feldspar and apatite, and for Ba in biotite (Icenhower and London, 1995, 1996). The porphyritic granodiorite and granite samples show parallel multi-element and REE patterns. Chondrite-normalized REE patterns (Fig. 6a) exhibit marked LREE enrichment and no significant Eu anomalies (Eu/Eu^* = 0.65–1.3). Primitive-mantle-normalized multi-element diagrams exhibit strong enrichment of Sr and Ba, and depletion of Nb, Ta, and other HFSEs (Fig. 6b).

4.2. Zircon U—Pb ages and trace element compositions

Zircon crystals from both porphyritic granodiorite and granite samples are mostly transparent, colorless to light brown, euhedral, and elongate prisms. CL images show clear oscillatory zoning (Fig. 7), and Th/U ratios are 0.14–0.71, typical of magmatic zircons (Belousova et al., 2002).

LA–ICP–MS U—Pb analyses of porphyritic granodiorite zircons yielded a weighted-mean $^{206}Pb/^{238}U$ age of 145.0 ± 1.9 Ma (MSWD = 2.3; Supplementary Table 2; Fig. 8a). Two early Paleozoic zircons with ages of 580.8 ± 9.2 and 424.8 ± 6.5 Ma were likely incorporated from wall-rocks during magma ascent. SHRIMP U—Pb dating of porphyritic granite zircons yielded a weighted-mean age of 145.9 ± 1.5 Ma (MSWD = 0.82; n = 10; Supplementary Table 3; Fig. 8b). A TEMORA 1 zircon was used for standardization of both LA–ICP–MS

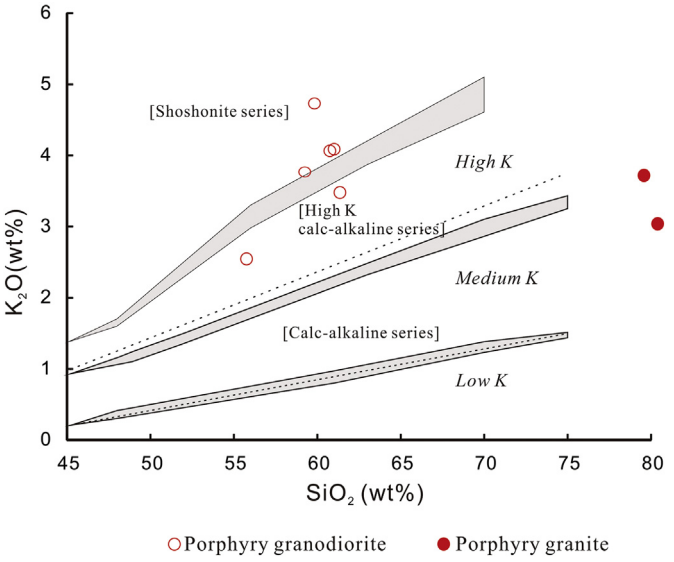

Fig. 4. K_2O–SiO_2 diagram for porphyritic granodiorite and granite of the Qiushuwan orefield. Dashed lines annotated in italics are after Le Maitre et al. (1989) and grey fields are after Rickwood (1989).

and SHRIMP analyses to ensure consistent results. As such, the porphyritic granodiorite and granite have identical zircon U—Pb ages, indicating they are likely to be coeval and possibly comagmatic in origin. In addition, the fact the ages for the Qiushuwan granite are within uncertainty of the age of the associated Cu—Mo mineralization (molybdenite Re—Os 146 ± 2 Ma; Guo et al., 2006) suggests they are genetically related.

The zircons from the porphyritic granodiorite contain 7.9–28 ppm Pb, have Th/U ratios of 0.15–0.31, ΣREE+Y contents of 1357–3132 ppm, and chondrite-normalized REE patterns that are characterized by heavy REE (HREE) enrichments and significantly positive Ce anomalies (Supplementary Table 4; Fig. 9), indicating they are magmatic zircons (Belousova et al., 2002). These zircons have $Ce^{(IV)}/Ce^{(III)}$ ratios, as calculated using a lattice strain model for the mineral–melt partitioning of Ce^{4+} and Ce^{3+}, between 43 and 515 (mean = 272). Zircons with $Ce^{(IV)}/Ce^{(III)}$ ratios of >200 most likely formed in a highly oxidized environment similar to those associated with the Cu-bearing porphyry deposits within northern Chile and the Tibetan area of China (Ballard et al., 2002; Liang et al., 2006), consistent with the oxidized environment suggested by the magnesian nature of these rocks (Section 4.1).

The crystallization temperatures of zircon from the porphyritic granodiorite are estimated to be 855 °C–1076 °C (mean = 941 °C) using the approach of Hayden and Watson (2007) with SiO_2 and TiO_2 activities of 1.0 and 0.6, respectively.

4.3. Whole-rock Sr—Nd and zircon Hf—O isotopic compositions

Whole-rock Rb—Sr and Sr—Nd isotopic compositions of two weakly silicified porphyritic granite and three porphyritic granodiorite samples have initial $^{87}Sr/^{86}Sr$ ratios and $\varepsilon_{Nd}(t)$ values in narrow ranges of 0.7056–0.7069 and −7.4 to −9.7, respectively (Supplementary Table 5). The rocks have model ages (T_{DM} = 973–719 Ma; T_{DM2} = 1724–1540 Ma) that are younger than the Paleoproterozoic to Mesoproterozoic basement material in this area as well as the Mesoproterozoic to Neoproterozoic supracrustal units of the Qinling Group (Shi et al., 2018). The Sr—Nd isotopic compositions of the Qiushuwan granites plot along an extension of the mantle array as shown in Fig. 10.

Porphyritic granodiorite zircons are characterized by $^{176}Hf/^{177}Hf$ ratios of 0.282511–0.282628, $\varepsilon_{Hf}(t)$ values of −2.49 to −5.13 (mean = −3.53), Hf model ages of 983–883 Ma, and T_{DM2} ages of 1491–1325 Ma (Supplementary Table 6). Zircon Hf isotopic compositions plot above the 1.5 Ga crustal evolution line ($^{176}Lu/^{177}Hf$ = 0.015) in an $\varepsilon_{Hf}(t)$–age diagram (Fig. 11a). The zircons have $\delta^{18}O$ values of +5.58‰ to +6.49‰ (mean = +6.00‰; Supplementary Table 7; Fig. 12). The fact that the precision of these analyses is better than ± 0.20‰ indicates that these zircon $\delta^{18}O$ values are slightly higher than the value expected for the mantle (5.3‰ ± 0.6‰; Valley et al., 2005).

5. Discussion

5.1. Petrogenesis

5.1.1. High-Ba–Sr signature of the Qiushuwan granites

The porphyritic granodiorite and granite units within the Qiushuwan orefield are metaluminous, high-K calc-alkaline to shoshonitic, and have trace element characteristics that are indicative of arc-type magmatism (Figs. 4, 6). The granitic rocks in the study area have Nb/Ta ratios between 9.6 and 17.5 (Supplementary Table 1), which are generally higher than the values expected for the continental crust (Taylor and Mclennan, 1995) but are similar to island arc volcanic rocks (Stolz et al., 1996), again supporting an arc-type affinity. Their high Ba (1300–3250 ppm) and Sr (929–1803 ppm) contents also indicate these are high-Ba–Sr granites (Fowler et al., 2008; Fig. 13a).

High-Ba–Sr granites were first identified by Tarney and Jones (1994). Unlike normal I-, S-, and A-type granites with generally low Ba and Sr contents, high-Ba–Sr granites are characterized by Ba and Sr contents of >500 and >300 ppm, respectively. They are commonly alkali-rich, with high K_2O contents and K_2O/Na_2O ratios, have low Nb and Ta contents, and highly fractionated REE patterns with small or no Eu anomalies (Fowler et al., 2008; Fowler and Henney, 1996). High-Ba–Sr granites are widespread in orogenic belts, but rarely found in modern subduction zones (Fowler et al., 2008). The high-Ba–Sr signature was commonly considered to have evolved from lithospheric mantle-derived mafic melts by fractional crystallization, accompanied by minor crustal contamination (Fowler et al., 2008; Fowler and Rollinson, 2012). However, some studies have argued that the high-Ba–Sr signature could arise via processes such as melting of source rocks with high Ba and Sr contents, magma mixing, fractional crystallization, assimilation and fractional crystallization, or interactions of silicic melts with the mantle (e.g., Liu et al., 2017). Other studies have emphasized the importance of melts derived from reworking of crustal materials in post-collisional tectonic settings (Choi et al., 2009; Lara et al., 2017).

Trace element characteristics of Qiushuwan porphyritic granodiorite and granite, such as the strongly fractionated REE patterns, depletion in heavy REEs and Y, and high Sr contents resemble those of adakite formed with residual garnet or amphibole (Fig. 13b, c; Martin, 1999). However, the high-K calc-alkaline to shoshonitic features of the granitic rocks are distinct from those of commonly sodic adakites of slab melting origin (Martin, 1999). Besides, their Ba/Sr ratios (0.77–2.98; mean = 2.13) are significantly higher than those of adakites (<0.5; Fowler et al., 2008). Therefore, these highly potassic porphyritic granodiorites and granites can be considered high-Ba–Sr granites (Fig. 13d).

5.1.2. Source of the Qiushuwan granites

The Qiushuwan porphyritic granodiorite and granite rocks have narrow ranges of initial $^{87}Sr/^{86}Sr$ ratios (0.7056–0.7069) and $\varepsilon_{Nd}(t)$ values (−7.4 to −9.7), which plot along an extension of the mantle array in the $(^{87}Sr/^{86}Sr)_i$–$\varepsilon_{Nd}(t)$ diagram (Fig. 10). Porphyritic granodiorite zircon Hf isotopic compositions also have a narrow range of $\varepsilon_{Hf}(t)$ values (−2.49 to −5.13).

Melting of lower continental crust with garnet residue may result in rocks with adakitic trace element signatures (Moyen, 2009). However, their Sr—Nd isotopic compositions are strikingly different to those of the lower crust (Jahn et al., 1999) and gneisses and amphibolites of

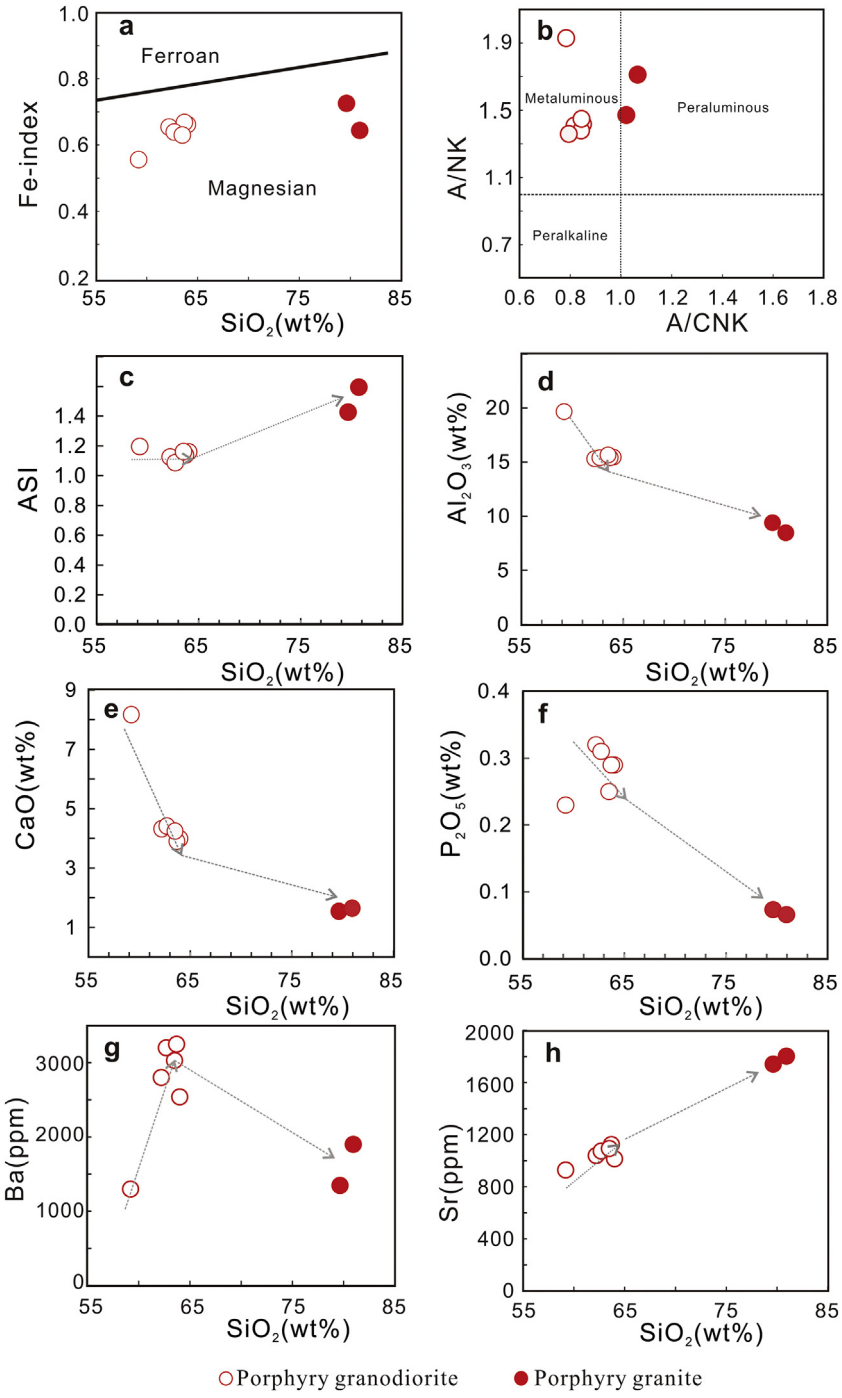

Fig. 5. Plots of (a) Fe-index–SiO_2 (after Frost and Frost, 2008), (b) A/NK–A/CNK, and (c–h) ASI, Al_2O_3, CaO, P_2O_5, Sr, and Ba vs SiO_2 for intrusions within the Qiushuwan area.

the Qinling Group (Fig. 10), and an over-thickened lower-crustal source for the granitic porphyries can thus be excluded, even though the rocks have model ages significantly older than their crystallization ages (whole-rock Nd T_{DM2} age = 1724–1540 Ma; zircon Hf T_{DM} age = 1491–1325 Ma). The porphyritic granodiorite zircon $\delta^{18}O$ values (+5.58‰ to +6.49‰) also differ from the compositions of the metamorphic rocks within the Qinling Group. Qinling Group rocks underwent peak metamorphism at 500–480 Ma and retrograde metamorphism at 470–450 Ma, and they have highly variable oxygen isotopic compositions. The whole-rock $\delta^{18}O$ values of the amphibolite and amphibole-bearing schists within this group range from 8.5‰ to 10.3‰ (Sun et al., 1997), whereas the felsic gneisses, garnet plagioclase amphibolites, and metamorphic mafic dikes in this group contain zircons with $\delta^{18}O$ values of 4.9‰–13.9‰, 5.94‰–8.38‰, and 5.44‰–13.4‰, respectively (Yu et al., 2016). Therefore, this excludes a lower-crustal origin for the Qiushuwan granites (Fig. 12). However, the consistent Sr–Nd–Hf–O isotopic compositions of the porphyritic granodiorite and granite indicate a common predominantly mantle source, possibly with minor assimilation of lower crust.

The porphyritic granodiorite and granite samples from the study area have decoupled Nd—Hf isotopic compositions, significantly different to those of the mantle array ($\varepsilon_{Hf}(t) = 1.55\varepsilon_{Nd}(t) + 1.21$) (Vervoort et al., 2011), with high positive Δ_{Hf} values ($\Delta_{Hf} = \varepsilon_{Hf}(t) - 1.55\varepsilon_{Nd}(t) - 1.21$) of +7.6 to +11.3 (Fig. 10b). Decoupling of Nd and Hf isotopes in river and oceanic sediments is likely caused by hydraulic sorting of minerals during transport. Selective deposition of zircons hosting

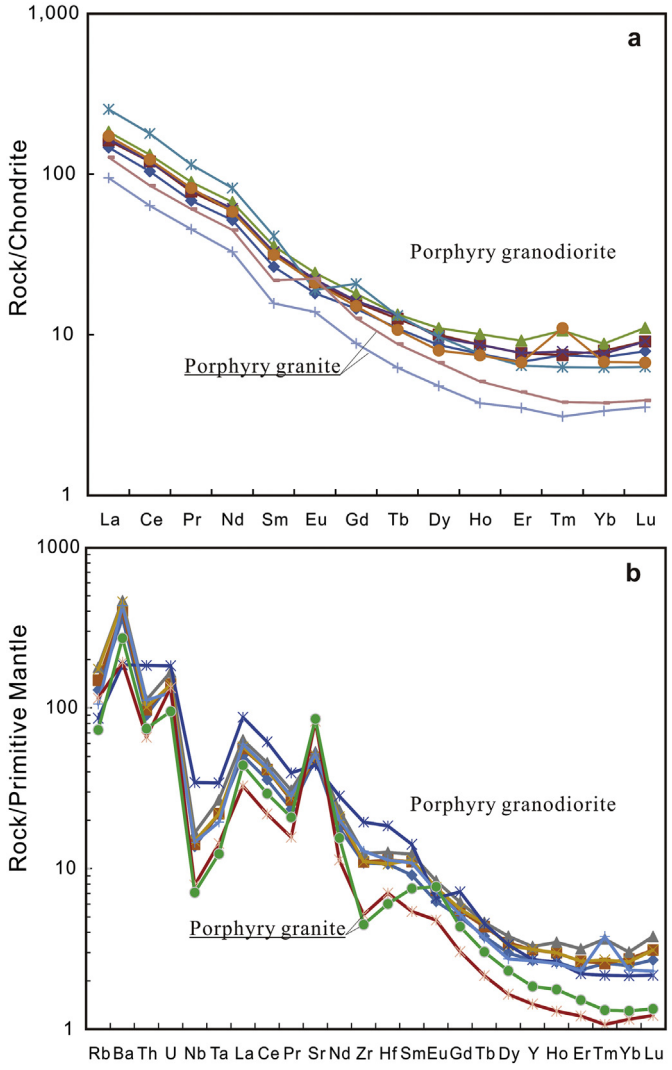

Fig. 6. (a) Chondrite-normalized REE and (b) primitive-mantle-normalized multi-element variation diagrams for granitic rocks in the study area normalized to the chondrite and primitive mantle compositions of Sun and McDonough (1989).

significant non-radiogenic Hf results in fine-grained and clay-dominated sediments with more radiogenic Hf (Vervoort et al., 2011). Recycling of oceanic sediments with anomalous Nd—Hf isotopic compositions into the mantle would have slowly shifted the overall isotopic composition of Earth's mantle towards a more radiogenic Hf composition (Garcon et al., 2013). Nd—Hf isotopic decoupling has been documented in many mantle-derived rocks (e.g., Park et al., 2017). Incorporation of zircon-barren oceanic sediments will also result in mantle sources with decoupled Nd—Hf isotopic signatures (Choi and Mukasa, 2012). In addition, high-Ba–Sr magmas are clearly associated with subduction-type environments, as documented by Thirlwall (1988) and Fowler et al. (2001). We therefore suggest that the decoupling of Nd and Hf isotopes in the porphyritic granodiorite and granite rocks in the study area indicates an important contribution from metasomatized lithospheric mantle. The relatively high zircon $\delta^{18}O$ values of the porphyritic granodiorite compared with mantle values is also consistent with assimilation of oceanic sediments in the mantle source (Zhu et al., 2017). This means that the granitic rocks in the study area most likely formed from magmas generated by partial melting of an enriched region of the subcontinental lithospheric mantle that was previously metasomatized by slab-derived fluids, with the resulting magmas assimilating minor amounts of lower-crustal material.

The existence of an enriched lithospheric mantle in the Mesozoic is supported by the presence of the Triassic Jiuzigou diopsidite–biotite diopsidite (235–233 Ma) with $\varepsilon_{Hf}(t)$ values of −0.84 to −8.41 (Gong et al., 2016) and Anwangshan pyroxenites with an $\varepsilon_{Nd}(t)$ value of −2.04 (Ren et al., 2019) in the western North Qinling Terrane, likely formed by partial melting of lithospheric mantle metasomatized by slab-derived fluids. A metasomatized subcontinental lithospheric mantle source was proposed for lamprophyre dikes along the Shangdan suture (*ca* 200 Ma), where time-integrated isotopic characteristics (ε_{Nd} (146 Ma) = −1.4 to −4.2; initial $^{87}Sr/^{86}Sr$ = 0.7036–0.7058) of the rocks (Wang et al., 2007) are slightly more radiogenic than those of granitic rocks in the Qiushuwan orefield. These lamprophyre dikes also have significantly high Ba (771–5132 ppm; mean = 2777 ppm) and Sr (465–1790 ppm; mean = 1019 ppm) contents, relatively low Rb contents (50.1–175 ppm; mean = 103 ppm), and highly fractionated REE patterns.

An enriched mantle origin for the Qiushuwan granitic rocks is also supported by their trace element compositions and the high magmatic temperatures recorded by the samples from the study area. These high-Ba–Sr granites plot in areas of Ba/La–Ba/Nb and La/Yb–Dy/Yb plots that are indicative of derivation from a predominantly enriched mantle source (Fig. 14a, b). The magmatic temperatures of the porphyritic granodiorites in the study area are estimated to be 855 °C–1076 °C as determined by Ti-in-zircon geothermometry (Hayden and Watson, 2007), similar to the 1050 °C–1100 °C homogenization temperatures for quartz-phenocryst-hosted melt inclusions within these granites

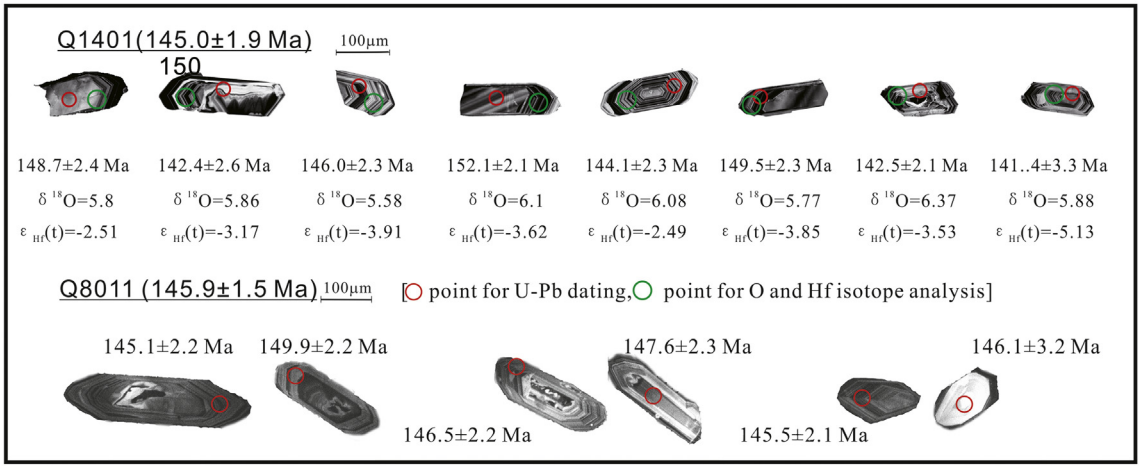

Fig. 7. Cathodoluminescence images of zircons from granodiorite (sample Q1401) and granite (sample Q8001) intrusions showing points for U—Pb, O, and Hf isotopic analyses.

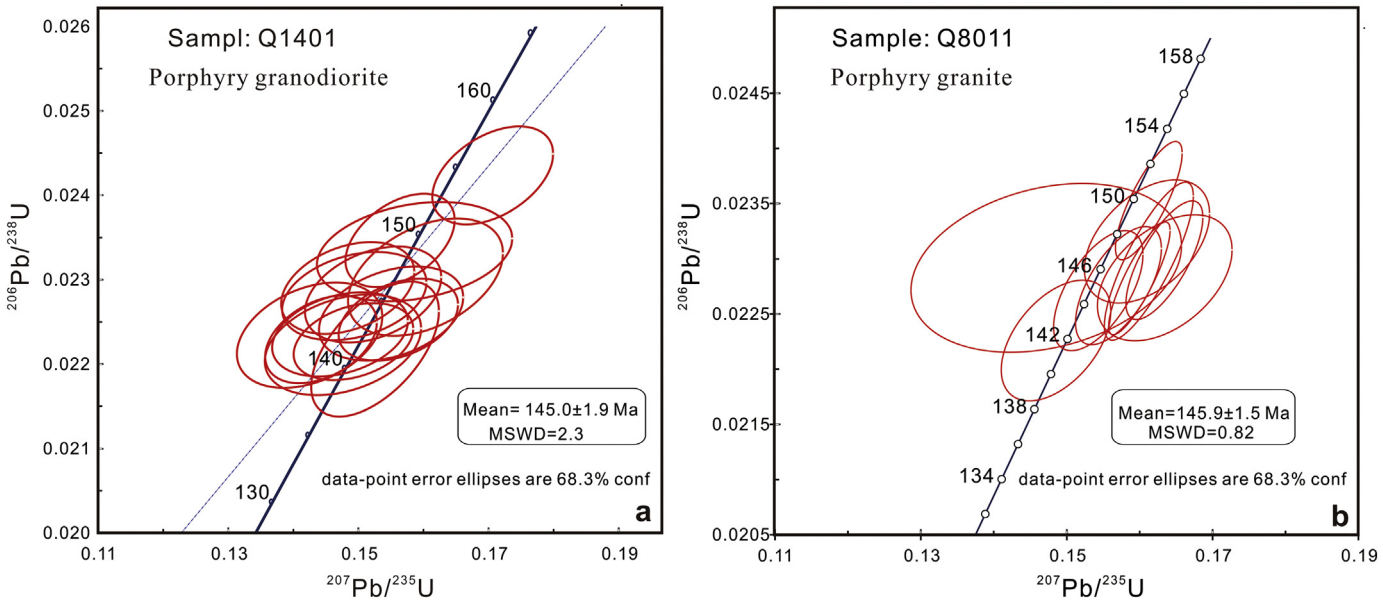

Fig. 8. Concordia diagrams for zircons from the porphyritic granodiorite and granite samples. (a) LA–ICP–MS U—Pb data for sample Q1401 (porphyritic granodiorite) and (b) SHRIMP U—Pb data for sample Q8001 (porphyritic granite).

(Wang et al., 2014b). The high magmatic temperatures recorded for these units are again consistent with a predominantly mantle origin.

5.1.3. Petrogenesis of the Qiushuwan granites

Even though the porphyritic granodiorite and granite units in the study area were most likely comagmatic and were both derived from enriched mantle sources, the variations in the major and trace element compositions within both the granites and the porphyritic granodiorites do not simply reflect fractional crystallization (Fig. 5). For instance, the positive correlations between Sr or Ba and SiO_2 contents within the porphyritic granodiorite are inconsistent with the high partition coefficients for these elements in plagioclase and biotite (Icenhower and London, 1995, 1996). The major and trace element variations within the granites might reflect source heterogeneity or variations in melting conditions. However, an alternative and possibly more plausible explanation is that early crystallized minerals such as plagioclase, biotite, and some K-feldspar formed a crystal mush that equilibrated with the residual melt within the system. The positive correlations between Sr or Ba and SiO_2 contents within the porphyritic granodiorite (Fig. 5g–h) could therefore reflect systematic increases in $D_{Sr}^{plagioclase/melt}$ and $D_{Ba}^{plagioclase/melt}$ values with increasing melt SiO_2 and H_2O concentrations during crystallization (Bedard, 2006). This is consistent with the >15 wt% SiO_2 gap in composition between the porphyritic granodiorite and the high-silica granites in the study area, as well as the major and trace element variation trends within these units, suggesting that the porphyritic granite represents the residual melt portion of the crystallizing magma within the study area (Fig. 5). This therefore suggests that the high-silica (~80 wt% SiO_2) porphyritic granite in the study area represents a highly evolved residual melt that was extracted from a crystallizing mush (Lee and Morton, 2015; Schaen et al., 2017) and crystallized at a shallow depth (Gualda and Ghiorso, 2013).

In summary, the whole-rock major and trace element and Sr—Nd isotopic compositions, and zircon Hf—O isotopic compositions, indicate

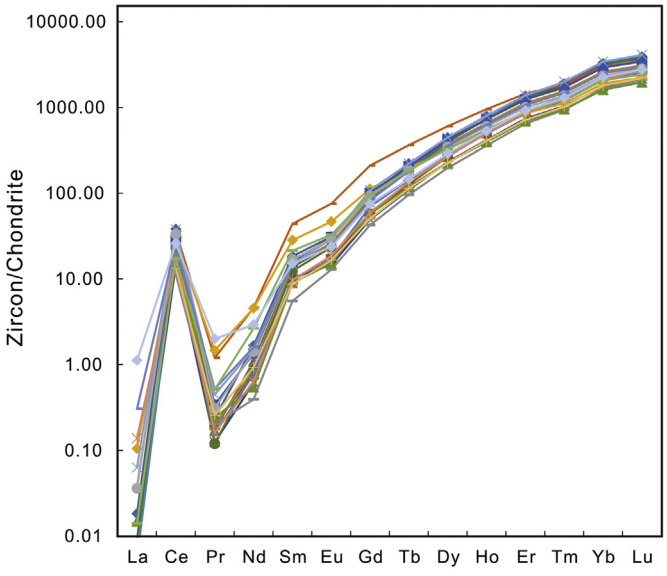

Fig. 9. Chondrite-normalized REE patterns for zircons from sample Q1401 (granodiorite porphyry) normalized to the chondrite composition of Sun and McDonough (1989).

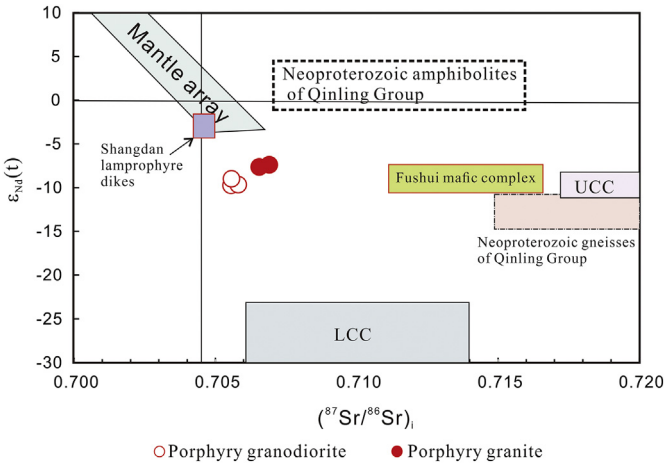

Fig. 10. $(^{87}Sr/^{86}Sr)_i$–$\varepsilon_{Nd}(t)$ plot for granitic porphyries from the Qiushuwan orefield. Fields for the upper continental crust (UCC) and lower continental crust (LCC) are from Jahn et al. (1999), and the mantle array is from Depaolo and Wasserburg (1979). Whole-rock Sr—Nd isotopic compositions of the Neoproterozoic Qinling Group and Fushui mafic complex (zircon U—Pb age of 488–484 Ma) are from Liu et al. (2013) and references therein, and Wang et al. (2014a), respectively. Sr—Nd isotopic composition for the Shangdan lamprophyre dikes (biotite ^{40}Ar—^{39}Ar plateau age of 219 ± 2 Ma) are from Wang et al. (2007). $(^{87}Sr/^{86}Sr)_i$ and $\varepsilon_{Nd}(t)$ values are based on $t = 146$ Ma.

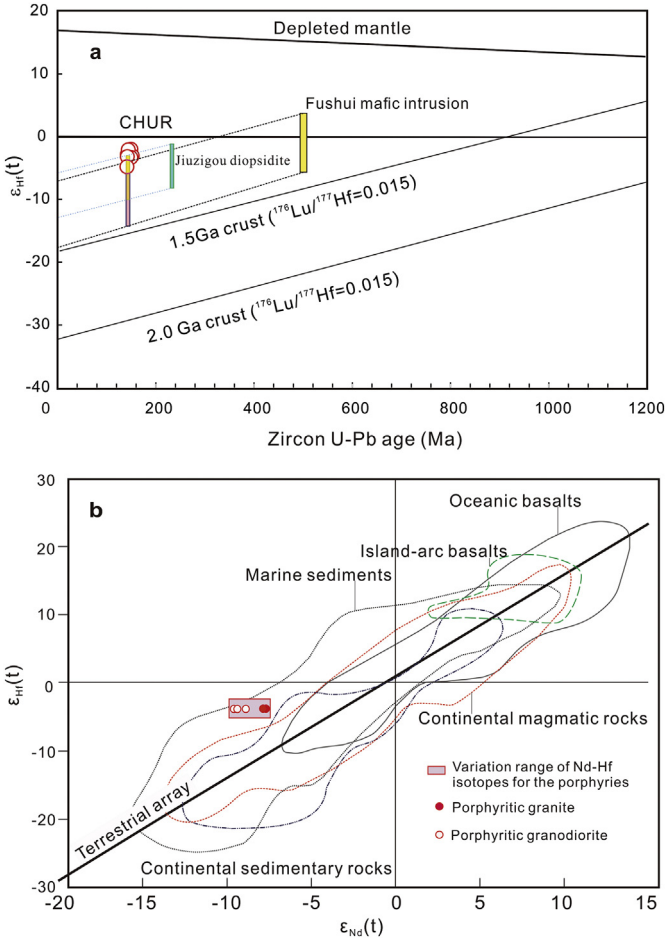

Fig. 11. Plots of (a) $\varepsilon_{Hf}(t)$–age for zircons from the porphyritic granodiorite and (b) $\varepsilon_{Nd}(t)$–$\varepsilon_{Hf}(t)$ for the porphyritic granodiorite and granite samples. Zircon Hf isotopic data for the Fushui mafic complex are from Shi et al. (2017) and data for the Jiuzigou diopsidite are from Gong et al. (2016). The zircon $\varepsilon_{Hf}(t)$ values of the porphyritic granite samples are assumed to be identical to those of the porphyritic granodiorite samples.

that the porphyritic granodiorite and granite rocks in the Qiushuwan Cu—Mo orefield are typical high-Ba–Sr granites, which might have derived from enriched subcontinental lithospheric mantle that had been

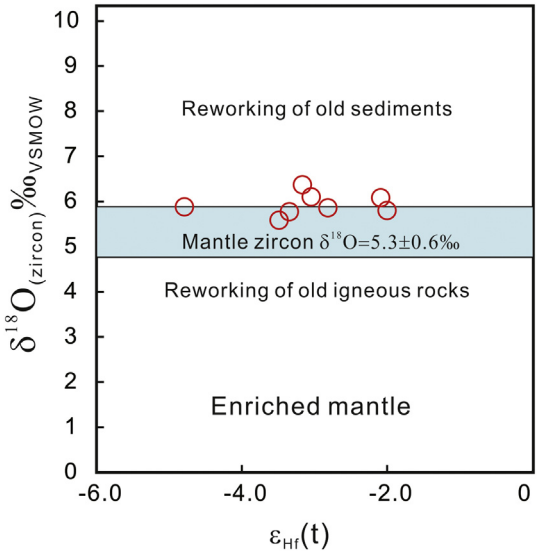

Fig. 12. $\delta^{18}O$–$\varepsilon_{Hf}(t)$ plot for zircons from the porphyritic granodiorite in the study area.

metasomatized by slab-derived fluids and then experienced assimilation of minor amounts of lower crust.

5.2. Tectonic setting

Integrated studies of paleomagnetism, sedimentation, and collision-related deformation and metamorphism have indicated that the oblique northwestward subduction of the YB began in the late Permian–Early Triassic with the scissor-like closure of the ocean basin, and continental collision propagating westward along the Mianlue suture during the Late Triassic (e.g., Liu et al., 2015; Wu and Zheng, 2013). Paleomagnetic data and sedimentary records of the northern Yangtze foreland basin indicate that the amalgamation of the NCC and YB did not cease until the Middle Jurassic. After collision in the Late Triassic, the whole Qinling orogenic belt (QOB) evolved into an intracontinental tectonic regime (Dong et al., 2016).

The early Mesozoic intracontinental collision resulted in an overthickened continental crust, and subsequent uplift and extensional tectonic collapse are suggested to have taken place in the Middle Jurassic (Qian et al., 2015) to Early Cretaceous (Hacker et al., 2000). Geophysical investigations indicate that the subduction-thickened continental lithosphere along the CCOB collapsed, and it is inferred that the orogenic root beneath the belt foundered into the asthenospheric mantle during the post-collisional stage (Guo and Chen, 2016; He and Zheng, 2018).

Late Mesozoic granites in the southern margin of the NCC may be derived mainly from partial melting of subducted YB continental crust (Bao et al., 2014). The recycling of subducted continental crust is supported by several lines of evidence including Nd—Hf (Bao et al., 2017), and Pb isotopic compositions of granites with crustal affinities at the northern YB margin (e.g., Zhao and Zheng, 2009).

As the final collision and amalgamation of the North and South China blocks occurred along the Mianlue suture, on the southern margin of the SQ, it seems reasonable to infer that YB crust accreted beneath the NQ (and probably the SQ) was removed prior to late Mesozoic granitic magmatism.

When and how the thickened lower crust was removed remains unclear. Delamination or collapse of thickened lower crust has been proposed as a mechanism for formation of adakite or adakitic granites in the QOB, with Late Triassic–Early Cretaceous ages (e.g., Zhang et al., 2016). Whether these events occurred during the Late Triassic *syn*-collisional period or Early Jurassic–Paleogene intracontinental orogeny is still unclear (Dong et al., 2016). He and Zheng (2018) suggested that the foundering of the subducted continental slab may have taken place in the Early Cretaceous on the basis of the extensive occurrence of magmatic and migmatitic rocks along the orogenic belt. However, with a predominant lithospheric mantle source for granitic rocks in the Qiushuwan orefield, the subducted YB continental crust was likely removed well before the Late Jurassic (Fig. 15). Furthermore, other late Mesozoic granites in the North and South Qinling terranes also exhibit high-Ba–Sr signatures with Sr–Nd–Hf isotopic compositions indicative of a significant mantle contribution, rather than a thickened lower crust or stagnated subducted continental crustal origin (Hu et al., 2017; Xie et al., 2015).

5.3. Implications for the distribution of mineralization within the East Qinling Orogenic Belt

The metals hosted by porphyry-type deposits are thought to be derived from the same source as the magmas that form the associated intrusion (Hedenquist and Lowenstern, 1994). Porphyry Cu and Cu—Mo deposits are also thought to be related to more oxidized magmas, whereas Mo mineralization is commonly associated with less oxidized magmas formed as a result of the remelting of continental crustal material (Oyarzun et al., 2001).

As discussed above, the granitic rocks within the Qiushuwan orefield are high-Ba–Sr granites derived mainly from an enriched region of the subcontinental lithospheric mantle (Fig. 14). The high temperature

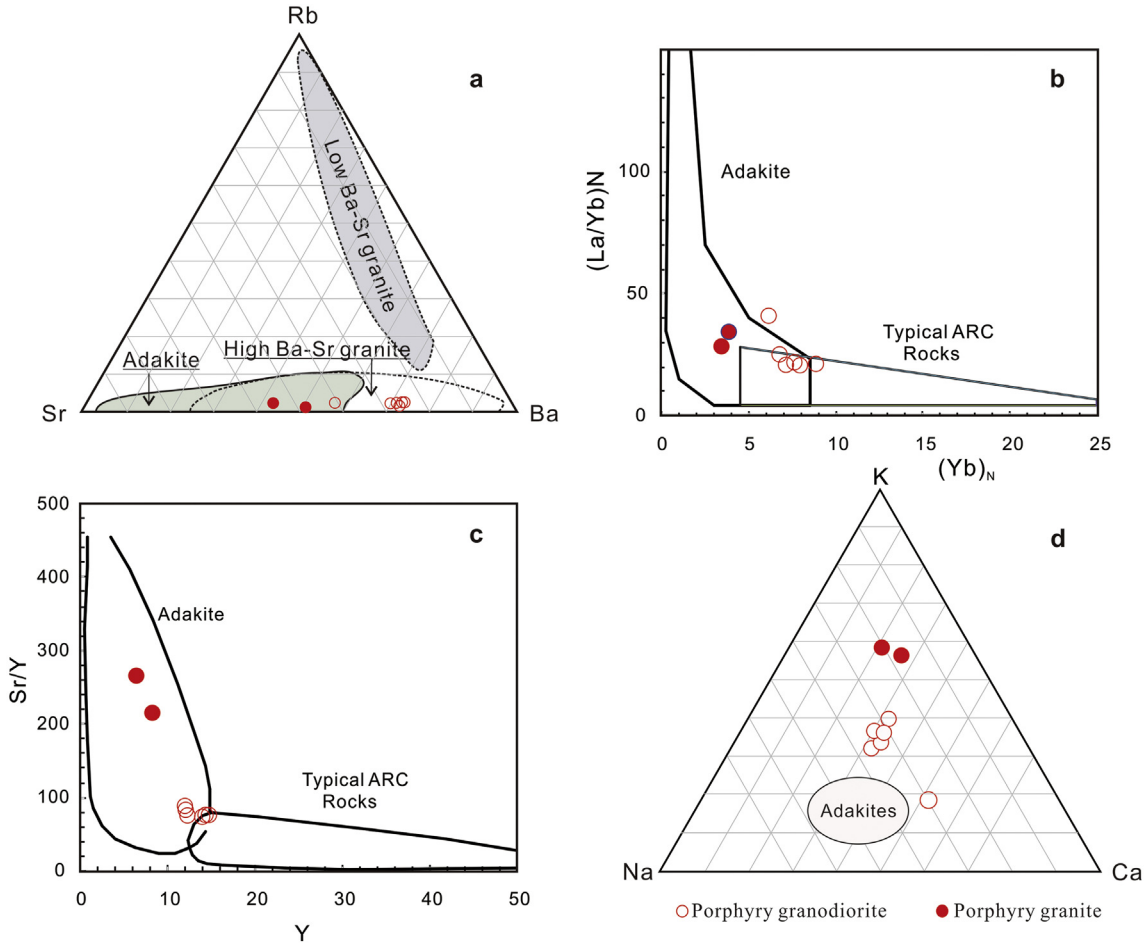

Fig. 13. Plots of Sr–Rb–Ba (a), $(La/Yb)_N$-$(Yb)_N$ (b), Sr/Y-Y (c), and Na–K–Ca (d) for the Qiushuwan high-Ba–Sr granites. Fields in the plots are from Lara et al. (2017) and Martin (1999).

(>850 °C), oxidized (zircon $Ce^{(IV)}/Ce^{(III)}$ ratios of 43–515), and hydrous nature of the magmas that formed the intrusions in the Qiushuwan orefield favor Cu mineralization. Magmatic sulfur only exists as sulfate (SO_4^{2-}) in oxidized magmas, leading to the delay or even prevention of sulfide saturation. The evolution of oxidized sulfate-bearing hydrous magmas involves the accumulation of chalcophile elements within melts during differentiation before these elements preferentially partition in exsolved magmatic–hydrothermal fluids during late-stage fluid exsolution events, with these fluids then forming late-stage hydrothermal Cu mineralization (Sun et al., 2013). In contrast, the late Mesozoic granites within the southern margin of the NCC generally formed from magmas generated by the partial melting of subducted YB continental crustal material (Bao et al., 2014), with the extensive Mo mineralization associated with these granites thought to be related to the fact they are derived from Mo-rich source rocks (Bao et al., 2017). This means that the uneven distribution of the late Mesozoic mineralization within the East Qinling orogenic belt reflects differences in magma source rocks, where Mo-rich continental crustal sources are related to the extensive Mo mineralization

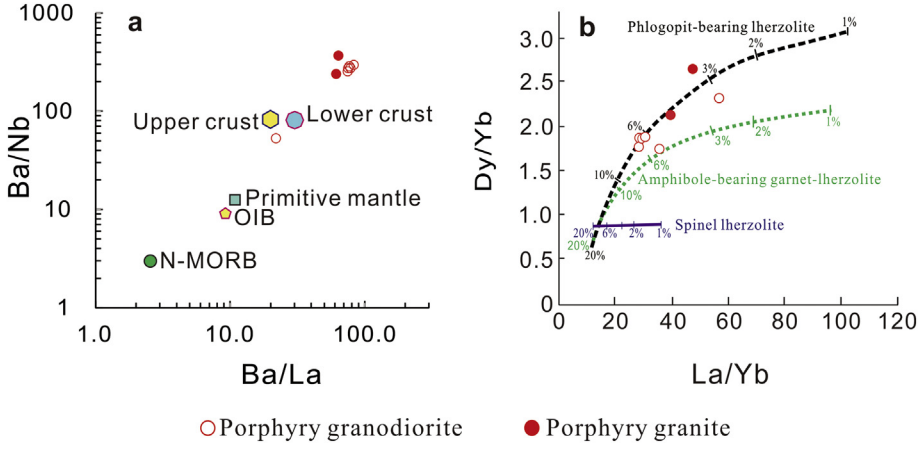

Fig. 14. (a) Ba/La–Ba/Nb and (b) La/Yb–Dy/Yb plots for the Qiushuwan granites. N-MORB, OIB, primitive mantle, lower crustal, and upper crustal fields are from Hofmann et al. (1986) and Sun and McDonough (1989). Parameters for the La/Yb–Dy/Yb plot are from Wang et al. (2014a) and references therein.

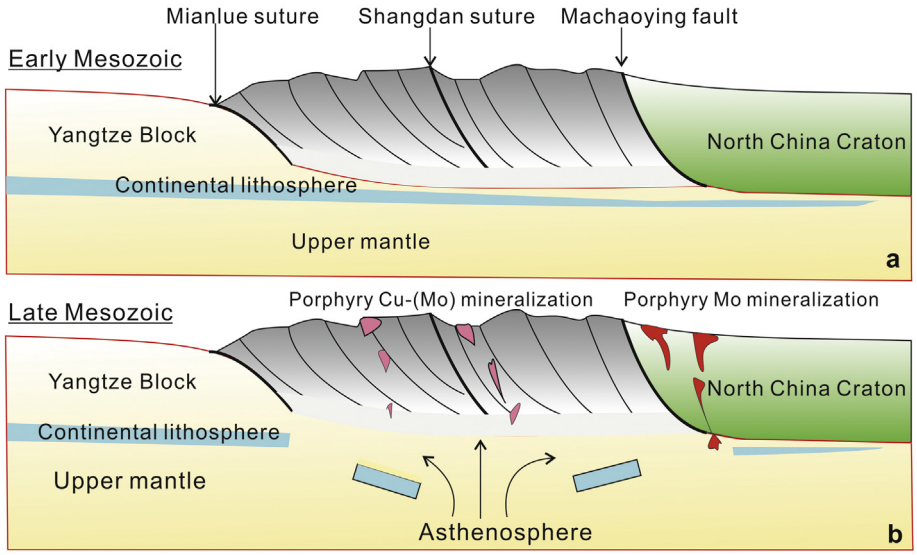

Fig. 15. Schematic diagram showing the effects of recycling of subducted continental crust of the Yangtze Block on the distribution of Mo—Cu mineralization in the East Qinling orogenic belt. (a) Subduction of continental crust in the early Mesozoic. (b) Heterogeneous removal of continental crust of the Yangtze Block containing abundant Mo-rich sedimentary rocks during the late Mesozoic post-collisional intracontinental orogeny. Partial melting of subducted continental crust stagnated beneath the southern margin of the North China Craton resulting in the late Mesozoic granite magmatism and associated Mo mineralization in a post-collisional tectonic setting. Upwelling of asthenospheric mantle led to partial melting of lithospheric mantle previously enriched through metasomatism by slab-derived fluids. This melting and subsequent assimilation of lower crust formed the high-Ba–Sr granitoids of the North and South Qinling terranes and related Cu-dominated porphyry mineralization.

in the southern margin of the NCC, and enriched lithospheric mantle sources are related to the Cu-dominated porphyry ore mineralization in the North Qinling terrane.

6. Conclusions

Ore-bearing porphyritic granodiorite and granite in the Qiushuwan Cu—Mo orefield in the North Qinling Terrane of the EQOB have ages of 145.0 ± 1.9 Ma (MSWD = 2.3) and 145.9 ± 1.5 Ma (MSWD = 0.82), respectively. The rocks are high-K calc-alkaline and shoshonitic, displaying magnesian and metaluminous to weakly peraluminous characteristics and trace element signatures typical of high-Ba–Sr granites. The narrow ranges of whole-rock initial $^{87}Sr/^{86}Sr$ ratios (0.7056–0.7069) and $\varepsilon_{Nd}(t)$ values (−7.4 to −9.7), and zircon $\varepsilon_{Hf}(t)$ (−2.49 to −5.13), $\delta^{18}O$ (+5.58‰ to +6.49‰), and positive Δ_{Hf} values (+7.61 to +11.3) indicate that the granitic rocks were likely derived mainly from partial melting of enriched subcontinental lithospheric mantle with minor assimilation of lower-crustal material. The mantle source produced a high-temperature (855–1076 °C) and oxidized (zircon $Ce^{(IV)}/Ce^{(III)}$ = 43–515) magma, which may account for the Cu-dominated ore mineralization. Therefore, the asymmetric distribution of Mo mineralization in the EQOB is probably due to the diversity of magma sources, with Mo-rich continental crust subducted beneath the North and South Qinling terranes likely having been removed before the Late Jurassic.

Supplementary data to this article can be found online at https://doi.org/10.1016/j.lithos.2019.105172.

Acknowledgements

This research was funded by the National Key R&D Program of China (Grant No. 2016YFC0600405) and NSFC Grant No. 41372083. We thank the chief editor Prof. Xianhua Li, Prof. Mike Fowler, and an anonymous reviewer for their constructive comments and helpful suggestions that significantly improved the manuscript.

References

Ballard, J.R., Palin, J.M., Campbell, I.H., 2002. Relative oxidation states of magmas inferred from Ce(IV)/Ce(III) in zircon: application to porphyry copper deposits of northern Chile. Contrib. Mineral. Petrol. 144, 347–364.

Bao, Z.W., Wang, C.Y., Zhao, T.P., Li, C.J., Gao, X.Y., 2014. Petrogenesis of the Mesozoic granites and Mo mineralization of the Luanchuan ore field in the East Qinling Mo mineralization belt, Central China. Ore Geol. Rev. 57, 132–153.

Bao, Z.W., Sun, W.D., Zartman, R.E., Yao, J.M., Gao, X.Y., 2017. Recycling of subducted upper continental crust: constraints on the extensive molybdenum mineralization in the Qinling-Dabie orogen. Ore Geol. Rev. 81, 451–465.

Bedard, J.H., 2006. Trace element partitioning in plagioclase feldspar. Geochim. Cosmochim. Acta 70, 3717–3742.

Belousova, E.A., Griffin, W.L., O'Reilly, S.Y., Fisher, N.I., 2002. Igneous zircon: trace element composition as an indicator of source rock type. Contrib. Mineral. Petrol. 143, 602–622.

Black, L.P., Kamo, S.L., Allen, C.M., Aleinikoff, J.N., Davis, D.W., Korsch, R.J., Foudoulis, C., 2003. TEMORA 1: a new zircon standard for Phanerozoic U-Pb geochronology. Chem. Geol. 200, 155–170.

Burnham, C.W., 1985. Energy-release in subvolcanic environments - implications for Breccia formation. Econ. Geol. 80, 1515–1522.

Chappell, B.W., White, A.J.R., 1992. I-Type and S-type granites in the lachlan fold belt. Trans. R. Soc. Edinb. Earth Sci. 83, 1–26.

Choi, S.H., Mukasa, S.B., 2012. Lu-Hf and Sm-Nd isotope systematics of Korean spinel peridotites: a case for metasomatically induced Nd-Hf decoupling. Lithos 154, 263–276.

Choi, S.G., Rajesh, V.J., Seo, J., Park, J.W., Oh, C.W., Pak, S.J., Kim, S.W., 2009. Petrology, geochronology and tectonic implications of Mesozoic high Ba-Sr granites in the Haemi area, Hongseong Belt, South Korea. Island Arc 18, 266–281.

Depaolo, D.J., Wasserburg, G.J., 1979. Petrogenetic mixing models and Nd-Sr isotopic patterns. Geochim. Cosmochim. Acta 43, 615–627.

Dong, Y.P., Santosh, M., 2016. Tectonic architecture and multiple orogeny of the Qinling Orogenic Belt, Central China. Gondw. Res. 29, 1–40.

Dong, Y.P., Yang, Z., Liu, X.M., Sun, S.S., Li, W., Cheng, B., Zhang, F.F., Zhang, X.N., He, D.F., Zhang, G.W., 2016. Mesozoic intracontinental orogeny in the Qinling Mountains, Central China. Gondw. Res. 30, 144–158.

Fowler, M.B., Henney, P.J., 1996. Mixed Caledonian appinite magmas: Implications for lamprophyre fractionation and high Ba-Sr granite genesis. Contrib. Mineral. Petrol. 126, 199–215.

Fowler, M., Rollinson, H., 2012. Phanerozoic sanukitoids from Caledonian Scotland: Implications for Archean subduction. Geology 40, 1079–1082.

Fowler, M.B., Henney, P.J., Darbyshire, D.P.F., Greenwood, P.B., 2001. Petrogenesis of high Ba-Sr granites: the Rogart pluton, Sutherland. J. Geol. Soc. London 158, 521–534.

Fowler, M.B., Kocks, H., Darbyshire, D.P.F., Greenwood, P.B., 2008. Petrogenesis of high Ba-Sr plutons from the Northern Highlands Terrane of the British Caledonian Province. Lithos 105, 129–148.

Frost, B.R., Frost, C.D., 2008. A geochemical classification for feldspathic igneous rocks. J. Petrol. 49, 1955–1969.

Gao, S., Luo, T.C., Zhang, B.R., Zhang, H.F., Han, Y.W., Zhao, Z.D., Hu, Y.K., 1998. Chemical composition of the continental crust as revealed by studies in East China. Geochim. Cosmochim. Acta 62, 1959–1975.

Garcon, M., Chauvel, C., France-Lanord, C., Huyghe, P., Lave, J., 2013. Continental sedimentary processes decouple Nd and Hf isotopes. Geochim. Cosmochim. Acta 121, 177–195.

Gong, X.K., Chen, D.L., Zhu, X.H., Dong, Z.C., Guo, C.L., 2016. The determination of Triassic ultramafic-syenite intrusive body and its geological significance, western North Qinling. Acta Petrol. Sin. 32, 177–192 (in Chinese with English abstract).

Gualda, G.A.R., Ghiorso, M.S., 2013. Low-pressure origin of high-silica rhyolites and granites. J. Geol. 121, 537–545.
Guo, Z., Chen, Y.J., 2016. Crustal structure of the eastern Qinling orogenic belt and implication for reactivation since the cretaceous. Tectonophysics 683, 1–11.
Guo, B.J., Mao, J.W., Li, H.M., Qu, W.J., Qiu, J.J., Ye, H.S., Li, M.W., Zhu, X.L., 2006. Re-Os dating of the molybdenite from the Qiushuwan Cu-Mo deposit in the east Qinling and its geological significance. Acta Petrol. Sin. 22, 2341–2348 (in Chinese with English abstract).
Hacker, B.R., Ratschbacher, L., Webb, L., McWilliams, M.O., Ireland, T., Calvert, A., Dong, S.W., Wenk, H.R., Chateigner, D., 2000. Exhumation of ultrahigh-pressure continental crust in east Central China: late Triassic-early Jurassic tectonic unroofing. J. Geophys. Res. Solid Earth 105, 13339–13364.
Hayden, L.A., Watson, E.B., 2007. Rutile saturation in hydrous siliceous melts and its bearing on Ti-thermometry of quartz and zircon. Earth Planet. Sci. Lett. 258, 561–568.
He, C.S., Zheng, Y.F., 2018. Seismic evidence for the absence of deeply subducted continental slabs in the lower lithosphere beneath the Central Orogenic Belt of China. Tectonophysics 723, 178–189.
Hedenquist, J.W., Lowenstern, J.B., 1994. The role of magmas in the formation of hydrothermal ore-deposits. Nature 370, 519–527.
Hofmann, A.W., Jochum, K.P., Seufert, M., White, W.M., 1986. Nb and Pb in oceanic basalts - new constraints on mantle evolution. Earth Planet. Sci. Lett. 79, 33–45.
Hu, H., Li, J.W., McFarlane, C.R.M., Luo, Y., McCarron, T., 2017. Textures, trace element compositions, and U-Pb ages of titanite from the Mangling granitoid pluton, East Qinling Orogen: Implications for magma mixing and destruction of the North China Craton. Lithos 284, 50–68.
Icenhower, J., London, D., 1995. An experimental study of element partitioning among biotite, muscovite, and coexisting peraluminous silicic melt at 200 MPa (H_2O). Am. Mineral. 80, 1229–1251.
Icenhower, J., London, D., 1996. Experimental partitioning of Rb, Cs, Sr, and Ba between alkali feldspar and peraluminous melt. Am. Mineral. 81, 719–734.
Jahn, B.M., Wu, F.Y., Lo, C.H., Tsai, C.H., 1999. Crust-mantle interaction induced by deep subduction of the continental crust: geochemical and Sr-Nd isotopic evidence from post-collisional mafic-ultramafic intrusions of the northern Dabie complex, Central China. Chem. Geol. 157, 119–146.
Lara, P., Oyhantcabal, P., Dadd, K., 2017. Post-collisional, late Neoproterozoic, high-Ba-Sr granitic magmatism from the Dom Feliciano Belt and its cratonic foreland, Uruguay: Petrography, geochemistry, geochronology, and tectonic implications. Lithos 277, 178–198.
Le Maitre, R.W., Bateman, P., Dudek, A., Keller, J.S., Lameyre, M., Le Bas, M.J., Sabine, P.A., Schmid, R., Sorensen, H., Streckeisen, A., Woolley, A.R., 1989. A Classification of Igneous Rocks and Glossary of Terms. Blackwell Scientific Publications, Oxford.
Lee, C.T.A., Morton, D.M., 2015. High silica granites: terminal porosity and crystal settling in shallow magma chambers. Earth Planet. Sci. Lett. 409, 23–31.
Li, X.H., Liang, X.R., Sun, M., Liu, Y., Tu, X.L., 2000. Geochronology and geochemistry of single-grain zircons: simultaneous in-situ analysis of U-Pb age and trace elements by LAM-ICP-MS. Eur. J. Mineral. 12, 1015–1024.
Li, X.H., Li, W.X., Li, Q.L., Wang, X.C., Liu, Y., Yang, Y.H., 2010a. Petrogenesis and tectonic significance of the similar to 850 Ma Gangbian alkaline complex in South China: evidence from in situ zircon U-Pb dating, Hf-O isotopes and whole-rock geochemistry. Lithos 114, 1–15.
Li, X.H., Long, W.G., Li, Q.L., Liu, Y., Zheng, Y.F., Yang, Y.H., Chamberlain, K.R., Wan, D.F., Guo, C.H., Wang, X.C., Tao, H., 2010b. Penglai zircon megacrysts: a potential new working reference material for microbeam determination of Hf-O isotopes and U-Pb age. Geostand. Geoanal. Res. 34, 117–134.
Li, X.H., Tang, G.Q., Gong, B., Yang, Y.H., Hou, K.J., Hu, Z.C., Li, Q.L., Liu, Y., Li, W.X., 2013. Qinghu zircon: a working reference for microbeam analysis of U-Pb age and Hf and O isotopes. Chin. Sci. Bull. 58, 4647–4654.
Liang, H.Y., Campbell, I.H., Allen, C., Sun, W.D., Liu, C.Q., Yu, H.X., Xie, Y.W., Zhang, Y.Q., 2006. Zircon Ce^{4+}/Ce^{3+} ratios and ages for Yulong ore-bearing porphyries in eastern Tibet. Miner. Deposita 41, 152–159.
Liu, B.X., Qi, Y., Wang, W., Siebel, W., Zhu, X.Y., Nie, H., He, J.F., Chen, F.K., 2013. Zircon U-Pb ages and O-Nd isotopic composition of basement rocks in the North Qinling Terrain, Central China: evidence for provenance and evolution. Int. J. Earth Sci. 102, 2153–2173.
Liu, S.F., Qian, T., Li, W.P., Dou, G.X., Wu, P., 2015. Oblique closure of the northeastern Paleo-Tethys in Central China. Tectonics 34. https://doi.org/10.1002/2014TC003784.
Liu, B., Ma, C.Q., Huang, J., Wang, L.X., Zhao, S.Q., Yan, R., Sun, Y., Xiong, F.H., 2017. Petrogenesis and tectonic implications of Upper Triassic appinite dykes in the East Kunlun orogenic belt, northern Tibetan Plateau. Lithos 284, 766–778.
Ludwig, K.R., 2003. Users Manual for Isoplot 3.00: A Geochronological Toolkit for Microsoft Excel. Berkeley Geochronology Center, Berkeley.
Mao, J.W., Pirajno, F., Xiang, J.F., Gao, J.J., Ye, H.S., Li, Y.F., Guo, B.J., 2011. Mesozoic molybdenum deposits in the east Qinling-Dabie orogenic belt: characteristics and tectonic settings. Ore Geol. Rev. 43, 264–293.
Martin, H., 1999. Adakitic magmas: modern analogues of Archaean granitoids. Lithos 46, 411–429.
Moyen, J.F., 2009. High Sr/Y and La/Yb ratios: the meaning of the "adakitic signature". Lithos 112, 556–574.
Oyarzun, R., Marquez, A., Lillo, J., Lopez, I., Rivera, S., 2001. Giant versus small porphyry copper deposits of Cenozoic age in northern Chile: adakitic versus normal calc-alkaline magmatism. Miner. Deposita 36, 794–798.
Park, K., Choi, S.H., Cho, M., Lee, D.C., 2017. Evolution of the lithospheric mantle beneath Mt. Baekdu (Changbaishan): Constraints from geochemical and Sr-Nd-Hf isotopic studies on peridotite xenoliths in trachybasalt. Lithos 286, 330–344.
Qian, T., Liu, S.F., Li, W.P., Gao, T.J., Chen, X.L., 2015. Early-Middle Jurassic evolution of the northern Yangtze foreland basin: a record of uplift following Triassic continent-continent collision to form the Qinling-Dabieshan orogenic belt. Int. Geol. Rev. 57, 327–341.
Ren, L., Bao, Z., Zhang, J., Li, K., Huang, W., Luo, Z., Liang, H., 2019. Magmatic response to slab tearing and resultant crustal evolution during scissor-like oblique continental collision: Insights from Triassic mafic and felsic intrusions in the Qinling orogen, China. Lithos 344–345, 68–85.
Rickwood, P.C., 1989. Boundary lines within petrologic diagrams which use oxides of major and minor elements. Lithos 22, 247–263.
Schaen, A.J., Cottle, J.M., Singer, B.S., Keller, C.B., Garibaldi, N., Schoene, B., 2017. Complementary crystal accumulation and rhyolite melt segregation in a late Miocene Andean pluton. Geology 45, 835–838.
Shi, Y., Pei, X.L., Castillo, P.R., Liu, X.J., Ding, H.H., Guo, Z.C., 2017. Petrogenesis of the similar to 500 Ma Fushui mafic intrusion and early Paleozoic tectonic evolution of the Northern Qinling Belt, Central China. J. Asian Earth Sci. 141, 74–96.
Shi, Y., Huang, Q.W., Liu, X.J., Krapez, B., Yu, J.H., Bai, Z.A., 2018. Provenance and tectonic setting of the supra-crustal succession of the Qinling complex: implications for the tectonic affinity of the North Qinling Belt, Central China. J. Asian Earth Sci. 158, 112–139.
Stolz, A.J., Jochum, K.P., Spettle, B., Hofmann, A.W., 1996. Fluid- and melt-related enrichment in the subarc mantle: evidence from Nb/Ta variations in island-arc basalts. Geology 24, 587–590.
Sun, S.S., McDonough, W.F., 1989. Chemical and Isotopic Systematics of Oceanic Basalts: Implications for Mantle Composition and Processes. pp. 313–345.
Sun, W.D., Zheng, Y.F., Li, S.G., Sun, Y., Zhang, G.W., 1997. An oxygen isotope study of contact metamorphic rocks from Songshugou in North Qinling. Acta Geol. Sin. 13, 162–167 (in Chinese with English abstract).
Sun, W.D., Liang, H.Y., Ling, M.X., Zhan, M.Z., Ding, X., Zhang, H., Yang, X.Y., Li, Y.L., Ireland, T.R., Wei, Q.R., Fan, W.M., 2013. The link between reduced porphyry copper deposits and oxidized magmas. Geochim. Cosmochim. Acta 103, 263–275.
Tanaka, T., Togashi, S., Kamioka, H., Amakawa, H., Kagami, H., Hamamoto, T., Yuhara, M., Orihashi, Y., Yoneda, S., Shimizu, H., Kunimaru, T., Takahashi, K., Yanagi, T., Nakano, T., Fujimaki, H., Shinjo, R., Asahara, Y., Tanimizu, M., Dragusanu, C., 2000. JNdi-1: a neodymium isotopic reference in consistency with LaJolla neodymium. Chem. Geol. 168, 279–281.
Tarney, J., Jones, C.E., 1994. Trace-element geochemistry of orogenic igneous rocks and crustal growth-models. J. Geol. Soc. London 151, 855–868.
Taylor, S.R., Mclennan, S.M., 1995. The geochemical evolution of the continental-crust. Rev. Geophys. 33, 241–265.
Thirlwall, M.F., 1988. Geochronology of late caledonian magmatism in Northern Britain. J. Geol. Soc. London 145, 951–967.
Valley, J.W., Lackey, J.S., Cavosie, A.J., Clechenko, C.C., Spicuzza, M.J., Basei, M.A.S., Bindeman, I.N., Ferreira, V.P., Sial, A.N., King, E.M., Peck, W.H., Sinha, A.K., Wei, C.S., 2005. 4.4 billion years of crustal maturation: oxygen isotope ratios of magmatic zircon. Contrib. Mineral. Petrol. 150, 561–580.
Vervoort, J.D., Plank, T., Prytulak, J., 2011. The Hf-Nd isotopic composition of marine sediments. Geochim. Cosmochim. Acta 75, 5903–5926.
Wang, X.X., Wang, T., Jahn, B.M., Hu, N.G., Chen, W., 2007. Tectonic significance of late Triassic post-collisional lamprophyre dykes from the Qinling Mountains (China). Geol. Mag. 144, 837–848.
Wang, H., Wu, Y.B., Li, C.R., Zhao, T.Y., Qin, Z.W., Zhu, L.Q., Gao, S., Zheng, J.P., Liu, X.M., Zhou, L., Zhang, Y., Yang, S.H., 2014a. Recycling of sediment into the mantle source of K-rich mafic rocks: Sr-Nd-Hf-O isotopic evidence from the Fushui complex in the Qinling orogen. Contrib. Mineral. Petrol. 168 (ARTN 1062).
Wang, L.L., Zhang, D.H., Tian, L., 2014b. Silicate melt inclusions in the Qiushuwan granitoids, northern Qinling belt, China: implications for the formation of a porphyry Cu-Mo deposit as a reduced magmatic system. C. R. Geosci. 346, 190–199.
Wiedenbeck, M., Hanchar, J.M., Peck, W.H., Sylvester, P., Valley, J., Whitehouse, M., Kronz, A., Morishita, Y., Nasdala, L., Fiebig, J., Franchi, I., Girard, J.P., Greenwood, R.C., Hinton, R., Kita, N., Mason, P.R.D., Norman, M., Ogasawara, M., Piccoli, R., Rhede, D., Satoh, H., Schulz-Dobrick, B., Skar, O., Spicuzza, M.J., Terada, K., Tindle, A., Togashi, S., Vennemann, T., Xie, Q., Zheng, Y.F., 2004. Further characterisation of the 91500 zircon crystal. Geostand. Geoanal. Res. 28, 9–39.
Williams, I.S., 1998. U-Th-Pb geochronology by ion microprobe. In: McKibben, M.A., Shanks, W.C., Ridley, W.I. (Eds.), Applications of Microanalytical Techniques to Understanding Mineralizing Processes, pp. 1–35.
Wu, Y.B., Zheng, Y.F., 2013. Tectonic evolution of a composite collision orogen: an overview on the Qinling-Tongbai-Hong'an-Dabie-Sulu orogenic belt in Central China. Gondw. Res. 23, 1402–1428.
Wu, F.Y., Yang, Y.H., Xie, L.W., Yang, J.H., Xu, P., 2006. Hf isotopic compositions of the standard zircons and baddeleyites used in U-Pb geochronology. Chem. Geol. 234, 105–126.
Xie, G.Q., Mao, J.W., Wang, R.T., Ren, T., Li, J.B., Da, J.Z., 2015. Origin of late Mesozoic granitoids in the newly discovered Zha-Shan porphyry Cu district, South Qinling, Central China, and implications for regional metallogeny. J. Asian Earth Sci. 103, 184–197.
Xie, G.Q., Mao, J.W., Wang, R.T., Meng, D.M., Sun, J., Dai, J.Z., Ren, T., Li, J.B., Zhao, H.J., 2017. Origin of the Lengshuigou porphyry-skarn Cu deposit in the Zha-Shan district, South Qinling, Central China, and implications for differences between porphyry Cu and Mo deposits. Miner. Deposita 52, 621–639.
Yang, L., Chen, F.K., Liu, B.X., Hu, Z.P., Qi, Y., Wu, J.D., He, J.F., Siebel, W., 2013. Geochemistry and Sr-Nd-Pb-Hf isotopic composition of the Donggou Mo-bearing granite porphyry, Qinling orogenic belt, Central China. Int. Geol. Rev. 55, 1261–1279.

Yu, H., Zhang, H.F., Li, X.H., Zhang, J., Santosh, M., Yang, Y.H., Zhou, D.W., 2016. Tectonic evolution of the North Qinling Orogen from subduction to collision and exhumation: evidence from zircons in metamorphic rocks of the Qinling Group. Gondw. Res. 30, 65–78.
Zhang, H., Ye, R.S., Liu, B.X., Wang, Y., Zhang, Y.S., Siebel, W., Chen, F.K., 2016. Partial melting of the South Qinling orogenic crust, China: evidence from Triassic migmatites and diorites of the Foping dome. Lithos 260, 44–57.
Zhao, Z.F., Zheng, Y.F., 2009. Remelting of subducted continental lithosphere: Petrogenesis of Mesozoic magmatic rocks in the Dabie-Sulu orogenic belt. Sci. China Ser. D Earth Sci. 52, 1295–1318.
Zhu, Y.S., Yang, J.H., Sun, J.F., Wang, H., 2017. Zircon Hf-O isotope evidence for recycled oceanic and continental crust in the sources of alkaline rocks. Geology 45, 407–410.